

Gain assistant control of photonic spin Hall effect

Muhammad Waseem,^{1,2} Muzamil Shah,^{3,4,*} and Gao Xianlong³

¹*Department of Physics and Applied Mathematics,*

Pakistan Institute of Engineering and Applied Sciences (PIEAS), Nilore 45650, Islamabad, Pakistan.

²*Center for Mathematical Sciences, PIEAS, Nilore, Islamabad 45650, Pakistan.*

³*Department of Physics, Zhejiang Normal University, Jinhua, Zhejiang 321004, China*

⁴*Zhejiang Institute of Photoelectronics and Zhejiang Institute for Advanced Light Source, Zhejiang Normal University, Jinhua, Zhejiang 321004, China*

(Dated: June 18, 2024)

In the photonic spin Hall effect (SHE), also known as transverse shift, incident light photons with opposite spins are spatially separated in the transverse direction due to the spin-orbit interaction of light. Here, we propose a gain-assisted model to control the SHE in the reflected probe light. In this model, a probe light is incident on a cavity containing a three-level dilute gaseous atomic medium, where the interaction between the atom and the control field follows two-photon Raman transitions. We show that the direction of photonic spin accumulations can be switched between positive and negative values across the Brewster angle in both the anomalous and normal dispersion regimes. For the same magnitude of control fields, the peak value of the photonic SHE is higher in the anomalous dispersion region compared to the normal dispersion regime. Additionally, the angular range around the Brewster angle is wider in the normal dispersion regime than in the anomalous dispersion region. Furthermore, the peak value of the photonic SHE and the angular range is controllable by changing the Rabi frequencies of the control fields and the probe field detuning. The measurement of photonic SHE based on gain assistance may enable spin-related applications such as optical sensing.

I. INTRODUCTION

The photonic spin Hall effect (SHE) is an optical phenomenon in which photons with opposite spins are separated from each other due to the spin-orbit interaction of light [1]. The SHE of light can be regarded as a direct optical analogy of SHE in an electronic system. In photonic SHE, photons' spin and refractive index gradient play a role similar to electrons spin and electric potential, respectively [2, 3]. This phenomenon can be traced back to the Imbert-Fedorov displacement [4, 5] and is time referred to as transverse shift. Recently, the photonic SHE has been intensively investigated in different physical systems. For example, in a static gravitational field [6], inside semiconductors via absorption [7], graphene layers [8–10], surface plasmon resonance systems [11–15], metamaterials [16], topological insulators [17], and two dimensional quantum materials [18, 19]. These studies highlight the SHE's unique properties and intriguing applications, such as probing topological phase transitions [18, 19], identifying graphene layers [8], chiral molecular detection [20], and performing mathematical operations and edge detection [21]. However, the photonic SHE typically appears on a nanometer scale, making direct measurement challenging. Experimental results using quantum weak measurements have shown that the SHE of light can be enhanced near the Brewster angle on reflection [22, 23].

However, in cavity quantum electrodynamics, the interaction between light and atoms induces atomic coherence and quantum interference effects. These coherence

and quantum interference effects led to many important phenomena, such as amplification without inversion [24], electromagnetically induced transparency [25], slow and fast light [26], quantum memory [27], optical solitons [28] and so forth. Another notable example is to manipulate the lateral shift known as the Goos-Hanchen (GH) effect of a light beam reflected or refracted from the interface of different media and structures [29–34].

In this paper, we studied photonic SHE using atomic coherence and quantum interference in cavity quantum electrodynamics. It has already been established that the dispersion absorption properties of an atomic medium can be modified using coherent control of the driving fields. Our motivation comes from an earlier work where a three-level atomic medium has been used via two-photon Raman transitions to obtain gain-assisted normal and anomalous light propagation [35, 36]. Following a similar scheme, we here study the behavior of the photonic SHE for the corresponding normal and also for the anomalous propagation of the light through the intracavity gain-assisted medium. Our results indicate that the direction of the photonic SHE can be switched between positive and negative values across the Brewster angle in both the anomalous and normal dispersion regions. We find out that the peak value of the photonic SHE can be externally controlled by adjusting the Rabi frequencies of the control fields and the detuning of the probe field, all without modifying the physical structure of the material. This flexible control of the peak value around the Brewster angle, in combination with weak measurement techniques [22], may offer a promising approach in cavity quantum electrodynamic systems.

The rest of the paper is organized as follows: Section II describes the physical system under considera-

* muzamill@zjnu.edu.cn

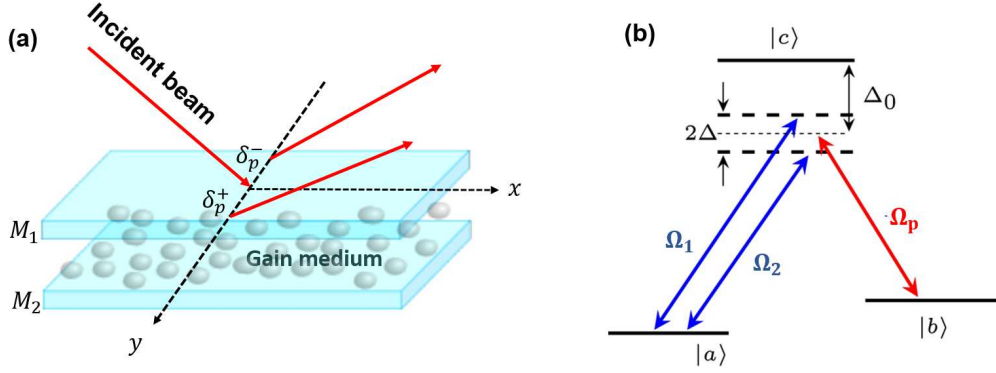


FIG. 1. (a) Schematic setup of a three-layer cavity system composed of two mirrors M_1 and M_2 containing a coherent Raman gain atomic medium in between them. Spin-dependent splitting occurs for a TM-polarized incident light reflected on mirror surface M_1 . (b) Energy level diagram of three-level Raman gains atomic medium driven by three lasers: probe field, and two driving fields.

tion and the corresponding mathematical expressions. Section III provides details of the results, plots, and discussions regarding the observed particular behaviors. Finally, the entire discussion of these interesting findings is summarized in Section IV.

II. THEORETICAL MODEL

Our proposed model is a cavity, which is composed of three layers as shown in Fig. 1(a). Layer 1 and 3 are the two dielectric mirrors M_1 and M_2 while layer 2 is intracavity three-level Raman gain medium trapped inside the two mirrors. In general, mirrors can also be replaced by a prism [34]. The thickness of each dielectric mirror is d_1 and the intracavity atomic gas medium is d_2 . The permittivities of each mirror are $\epsilon_1 = 2.2$, whereas the permittivity of atomic medium is ϵ_2 . The permittivity of the intracavity medium can be defined in terms of its dielectric susceptibility as [30]

$$\epsilon_2 = 1 + \chi, \quad (1)$$

where χ is a complex quantity, represents the dielectric susceptibility of the intracavity Raman gain medium, and can be expressed as

$$\chi = \chi_1 + i\chi_2, \quad (2)$$

where, real part χ_1 represents dispersion and imaginary part χ_2 represents the absorption of the probe field.

In order to obtain the dielectric susceptibility of the intracavity medium, we consider the Λ -type atomic system having an excited state $|c\rangle$ and two ground states $|a\rangle$ and $|b\rangle$ as shown in Fig. 1(b). Two control laser fields of amplitude E_1 and E_2 with frequencies ν_1 and ν_2 interacts for off-resonantly with atomic transition $|a\rangle \leftrightarrow |c\rangle$. Initially, the atoms are prepared in state $|a\rangle$ using optical pumping. The probe field is applied across the transition $|b\rangle \leftrightarrow |c\rangle$ with amplitude E_p and frequency ν_p . The energy levels $|b\rangle$ and $|c\rangle$ are not populated.

The effective Hamiltonian of the system can be written as

$$H = H_0 + H_1, \quad (3)$$

where the unperturbed part of the Hamiltonian is

$$H_0 = -\hbar\omega_{ca}|a\rangle\langle a| - \hbar\omega_{cb}|b\rangle\langle b|. \quad (4)$$

Here $\omega_{ca} = 2\pi\nu_{ca}$ and $\omega_{cb} = 2\pi\nu_{cb}$ are the angular frequencies corresponding to the respective atomic transitions. The perturbed part of the Hamiltonian is

$$H_1 = -\hbar(\Omega_1 e^{-i\omega_1 t} + \Omega_2 e^{-i\omega_2 t})|c\rangle\langle a| - \hbar\Omega_p e^{-i\omega_p t}|c\rangle\langle b| - h.c., \quad (5)$$

Here, $\omega_1 = 2\pi\nu_1$, $\omega_2 = 2\pi\nu_2$ and $\omega_p = 2\pi\nu_p$ are the angular frequencies associated with the driving laser field E_1 , E_2 and probe field E_p , respectively. The corresponding Rabi frequencies are $\Omega_1 = \mu_{ca}|E_1|/\hbar$, $\Omega_2 = \mu_{ca}|E_2|/\hbar$, and $\Omega_p = \mu_{cb}|E_p|/\hbar$. We consider that the driving laser fields E_1 and E_2 are strong fields while the probe field E_p is a weak field, which means $|\Omega_1||\Omega_2| \gg |\Omega_p|$. Using the definition of dielectric polarization and following the density matrix approach [37], the dielectric susceptibility for the Raman gain process can be written as

$$\chi = \frac{M_1}{(\delta_p - \Delta\nu) + i\Gamma} + \frac{M_2}{(\delta_p + \Delta\nu) + i\Gamma}, \quad (6)$$

where $\delta_p = \nu_p - \nu_0$ is the probe field detuning and $\nu_0 = \nu_1 - \nu_{ca} + \nu_{cb}$. The Raman transition inverse lifetime is Γ , which represents the spectral width of two gain lines. The driving fields E_1 and E_2 are detuned from each other by an amount $2\Delta\nu$, where $\Delta\nu$ is the difference between ν_1 and ν_2 . We define

$$M_j = N \frac{|\mu_{cb}|^2 |\Omega_j|^2}{4\pi\hbar\epsilon_0 \Delta_0^2}, \quad (7)$$

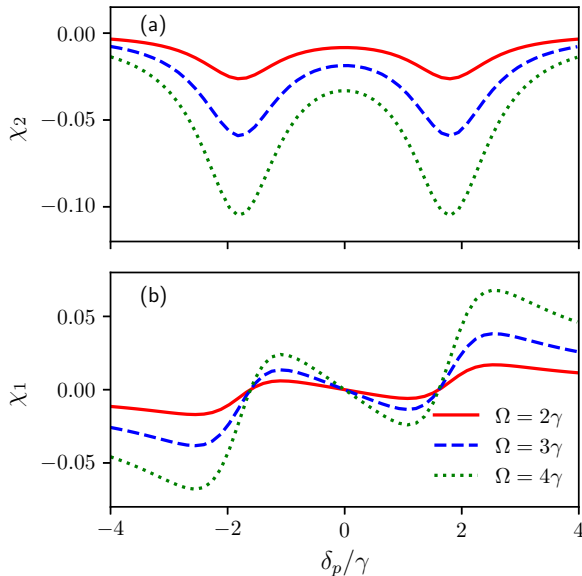


FIG. 2. (a) Absorption spectrum and (b) Dispersion spectrum of the weak probe field as a function of probe detuning δ_p/γ at different values of control fields $\Omega = \Omega_1 = \Omega_2$. The region at resonance $\delta_p = 0$ is called the anomalous dispersion regime while the region at $\delta_p = \Delta\nu = 1.8\gamma$ is called the normal dispersion region. The others parameters are $\Gamma = 0.8\gamma$, $\Delta_1 = 5\gamma$, $\Delta_p = 4.9\gamma$, $\mu_{cb} = 3.79 \times 10^{-29}$, $\epsilon_0 = 8.85 \times 10^{-12}$, $N = 10^{12}/\text{cm}^3$, and $\lambda = 852 \text{ nm}$, where $\gamma = 10^6 \text{ Hz}$.

where $j = 1, 2$, N is the number density of the atom, and μ_{cb} is the dipole matrix element of the transition $|c\rangle \leftrightarrow |b\rangle$. The common detuning is $\Delta_0 = (\Delta_1 + \Delta_p)/2$ with $\Delta_1 = 2\pi(v_1 - v_{ca})$ and $\Delta_p = 2\pi(v_p - v_{cb})$. We consider the condition that $\Delta_0 \gg \Delta_1 - \Delta_p$. It is clear from Eq. (6) that the susceptibility of the Raman gains medium and hence its permittivity ϵ_2 can be modified and controlled by changing several parameters such as the Rabi frequencies of the driving fields Ω_1 and Ω_2 and the probe field detuning δ_p .

We consider that a TE and TM-polarized probe light beam is incident on the cavity mirror M_1 from the vacuum with an angle of incidence θ_i . This monochromatic Gaussian probe beam will be reflected at the structure interface or pass through the structure. After reflection, the left- and right circular polarization components of the incident light beam will be spatially separated in the direction perpendicular to the plane of incidence (y-axis) as shown in Fig. 1(a). This perpendicular shift is known as the photonic SHE. The photonic SHE is inherently a polarization-dependent optical phenomenon of incident light in which photons with opposite helicity are separated from each other due to the spin-orbit interaction of light. The photonic SHE can be considered as an optical version of the electron SHE [38]. For the three-layer structure discussed here, the complex reflection coefficients for TM polarized r_p and TE-polarized

r_s can be written as [15]

$$r_{p,s} = \frac{r_{p,s}^{12} + r_{p,s}^{23} e^{2ik_2z d}}{1 + r_{p,s}^{12} r_{p,s}^{23} e^{2ik_2z d}}, \quad (8)$$

where $r_{p,s}^{ij}$ is the Fresnel's reflection coefficient at the $i - j$ interface given by

$$r_p^{ij} = \frac{k_{iz}/\epsilon_i - k_{jz}/\epsilon_j}{k_{iz}/\epsilon_i + k_{jz}/\epsilon_j}, r_s^{ij} = \frac{k_{iz} - k_{jz}}{k_{iz} + k_{jz}}.$$

Here $k_{iz} = \sqrt{k_0^2 \epsilon_i - k_x^2}$ represents the normal wave vector in the corresponding layer, and $k_x = \sqrt{\epsilon_1} k_0 \sin \theta_i$ is the wave vector along the x direction. Here, $k_0 = 2\pi/\lambda$ denotes the wave vector with λ being the light wavelength. It can be seen from Eq. (8) that reflection coefficients depend on gain medium permittivity ϵ_2 which can be effectively controlled through manipulation of χ . This leads to controllable photonic SHE of light. Having calculated the dielectric susceptibility for the Raman gain process, we can calculate the photonic SHE in terms of Fresnel's reflection coefficients. The corresponding transverse spin-displacements δ_p^+ and δ_p^- can be expressed in terms of the reflective coefficients of the three-layer atomic system [13, 14]:

$$\delta_p^\pm = \mp \frac{k_1 w_0^2 \text{Re} \left[1 + \frac{r_s}{r_p} \right] \cot \theta_i}{k_1^2 w_0^2 + \left| \frac{\partial \ln r_p}{\partial \theta_i} \right|^2 + \left| \left(1 + \frac{r_s}{r_p} \right) \cot \theta_i \right|^2}. \quad (9)$$

Here $k_1 = \sqrt{\epsilon_1} k_0$ and w_0 represents the radius of the waist of the incident beam.

III. RESULTS AND DISCUSSION

Based on the fact that the optical properties of the Raman medium can be controlled, we now discuss the results of the photonic SHE of the reflected probe beam, which can be modified and controlled. To do so, we first consider the susceptibility analysis with $\Omega_1 = \Omega_2 = \Omega$ which consequently gives $M_1 = M_2$. We choose the parameters related to Cs vapors used in experiment [35]. These parameters are $\Gamma = 0.8\gamma$, $\Delta\nu = 1.8\gamma$, $\Delta_1 = 5\gamma$, $\Delta_p = 4.9\gamma$, $\mu_{cb} = 3.79 \times 10^{-29} \text{ Cm}$, $\epsilon_0 = 8.85 \times 10^{-12} \text{ Fm}^{-1}$, $N = 10^{12}/\text{cm}^3$, and $\lambda = 852 \text{ nm}$, where $\gamma = 10^6 \text{ Hz}$. The interaction length of the atomic medium is $d = 100 \text{ nm}$. The corresponding dielectric permittivities of the two mirrors are $\epsilon_1 = 2.22$, $\epsilon_3 = 2.22$. We first plot the imaginary and real parts of χ as a function of probe detuning δ_p in Fig. 2(a) and (b), respectively. The imaginary part shows the absorption, while the real component exhibits the dispersion of the probe field. It must be noted that when the incident probe field interacts resonantly with the Raman gain medium, then the medium experiences zero dispersion and a small amount of gain. The amount of gain increases as the strength of Ω increases while dispersion does not depend on it. This region is known as the

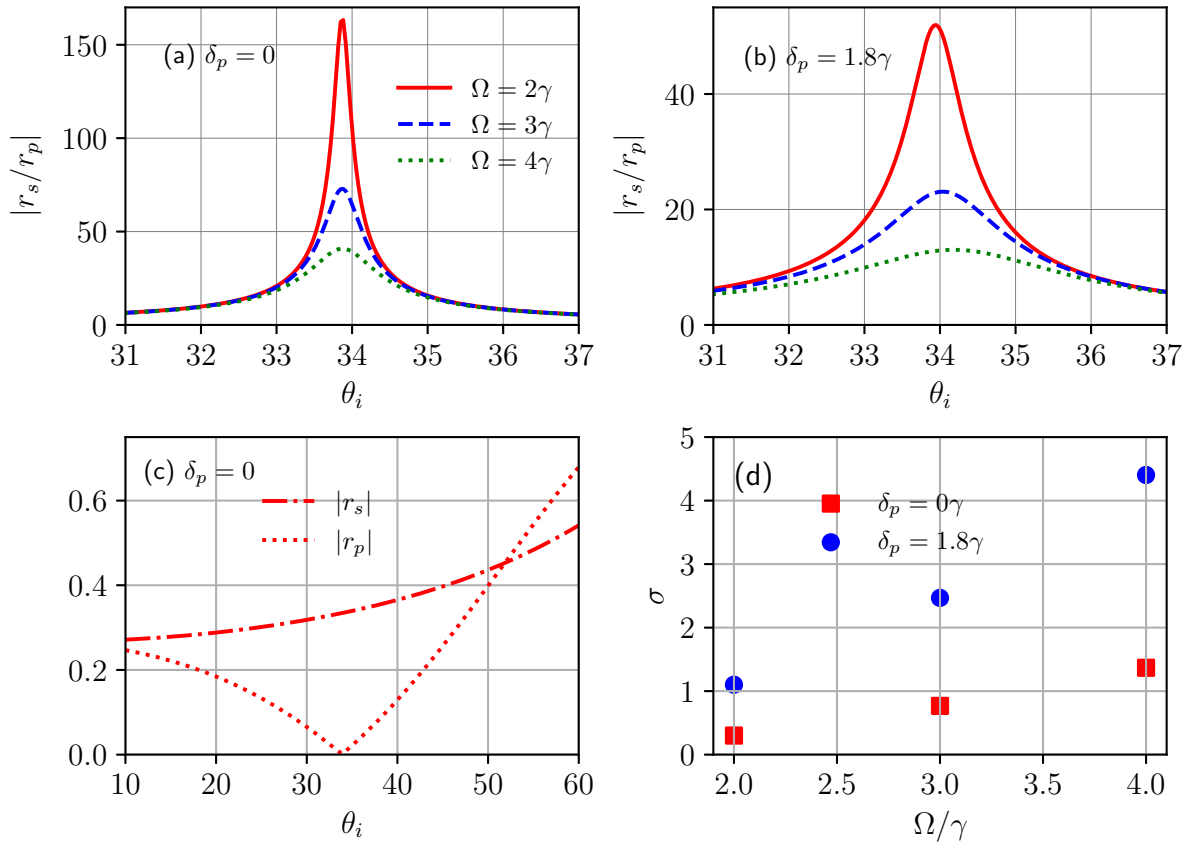


FIG. 3. Ratio of $|r_s/r_p|$ as a function of incident angle θ_i in the (a) anomalous dispersion region at $\delta_p = 0$ and (b) normal dispersion region at $\delta_p = 1.8\gamma$ at three different values of $\Omega = 2\gamma$ (solid), $\Omega = 3\gamma$ (dashed), and $\Omega = 4\gamma$ (dotted). (c) Plot of individual $|r_s|$ and $|r_p|$ as a function of incident angle θ_i in the anomalous dispersion region at $\delta_p = 0$. At Brewster angle θ_b reflection coefficient r_p converge to zero, which results the enhancement of ratio $|r_s/r_p|$. (d) Full-width half maximum σ as a function of Ω in anomalous dispersion region (squares) and normal dispersion region (circles). We consider the Interaction length of the atomic medium $d = 100$ nm. The dielectric permittivities of two mirrors are $\epsilon_1 = 2.22$, $\epsilon_3 = 2.22$. The rest of the parameters are the same as for Fig. 2.

anomalous dispersion region. Slightly away from resonance and between the two Raman gain doublet, the probe field dispersion becomes negative. At detuning $\Delta\nu = 1.8\gamma$, the dispersion again becomes zero with a larger gain and this region is known as the normal dispersion region. In this way, the optical response of the Raman gain medium can be obviously controlled and this is the motivation of using this system to coherently control the photonic SHE in this work.

It is evident from the Eq. (9), transversal shift δ_p depends on the ratio r_s to r_p for an arbitrary incident angle. Its value larger than one can give rise to a noticeable transverse shift. Therefore, we plot the ratio of $|r_s/r_p|$ as a function of the incident angle θ_i in the anomalous dispersion region at $\delta_p = 0$ shown in Fig. 3 (a) and the normal dispersion region at $\delta_p = 1.8\gamma$ shown in Fig. 3(b). The solid, dashed, and dotted curves correspond to $\Omega = 2\gamma$, $\Omega = 3\gamma$, and $\Omega = 4\gamma$, respectively. The peak value of $|r_s/r_p|$ for the anomalous dispersion region is three times higher than the normal dispersion

region. The ratio increases significantly in the vicinity of the Brewster angle $\theta_B \approx 33.9^\circ$ for both normal and anomalous dispersion regions. The reason is that $|r_p|$ response vanishes at Brewster angle as shown by the dotted curve in Fig 3(c) for the case of $\delta_p = 0$. This disappearing response of $|r_p|$ results in the enhancement of $|r_s/r_p|$. From the spectrum of $|r_s/r_p|$ shown in Fig. 3 we extract the full width half maximum σ , which quantify the angular range of $\theta_i \in [0^\circ, 89^\circ]$ over which $|r_s/r_p| \gg 1$. In Fig 3(d), squares and circles show the values of σ versus Ω for anomalous and normal dispersion, respectively. Clearly angular range increased with the increase of Ω and became wider for the normal dispersion regime compared to the normal dispersion regime. In other words, the result in Fig. 3(d) validates that $|r_s/r_p| \gg 1$ can be achieved in a very wide angular range by exploiting the anomalous dispersion regime. These results also indicate that when the angular range is wider, the peak value of $|r_s/r_p|$ decreases and vice versa.

Next, we analyze the transverse shift due to the pho-

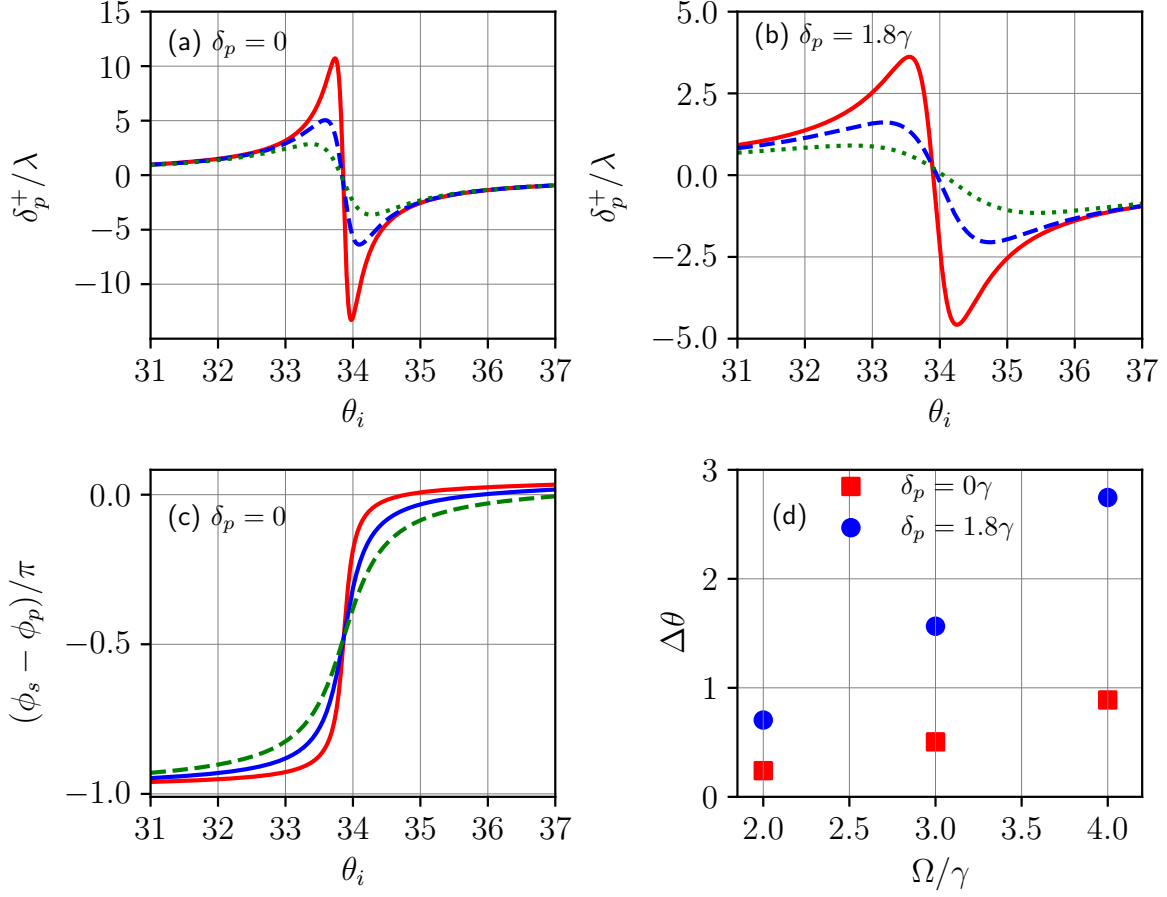


FIG. 4. (a) Photonic spin Hall shift δ_p^+ as a function of incident angle θ_i in the (a) anomalous dispersion region at $\delta_p = 0$ and (b) normal dispersion region at $\delta_p = 1.8\gamma$ at three different values of $\Omega = 2\gamma$ (solid), $\Omega = 3\gamma$ (dashed), and $\Omega = 4\gamma$ (dotted). (c) The phase difference $\phi_s - \phi_p$ in the anomalous dispersion region experiences a π phase variation across the Brewster angle, and the spin accumulation reverses its directions accordingly. (d) Angular width $\Delta\theta = \theta^- - \theta^+$ of incident angle as a function of Ω in anomalous dispersion region (squares) and normal dispersion region (circles). Angular width $\Delta\theta$ shows the range of incident angle over which photonic spin Hall shift changes sign from positive to negative. The rest of the parameters are the same as for Fig. 3

tonic SHE. We only presented the transverse shift of the right circularly polarized photon spin-dependent component δ_p^+ because the beam shifts for the two circular components are equal in magnitude and opposite in sign. We plot the photonic spin Hall shift δ_p^+/λ as a function of the incident angle θ_i in the anomalous dispersion region at $\delta_p = 0$ shown in Fig. 4(a) and normal dispersion region at $\delta_p = 1.8\gamma$ shown in Fig. 4(b). For clarity, we consider the three different values of control field $\Omega = 2\gamma$ (solid) $\Omega = 3\gamma$ (dashed), and $\Omega = 4\gamma$ (dotted) in order to make one-to-one correspondence with results of $|r_s/r_p|$ in Fig. 3. It is shown that δ_p^+ give extreme values in the vicinity of θ_B where r_s/r_p is large. The results indicate that with the increase of the control field Ω , the maximum positive and negative spin shift values keep on decreasing and their positions shift almost near the Brewster angle. This decrease of δ_p^+ is related to dielectric constant ϵ_2 or susceptibility

χ . From the results shown in Fig. 2, the probe susceptibility is purely imaginary at anomalous and normal dispersion regimes and decreases with ω , which results in a decrease in the magnitude of shift [15]. The transverse shift changes the sign from positive to negative around the Brewster angle θ_B . The transverse SHE is positive for $\theta_i < \theta_b$, negative for $\theta_i > \theta_b$, and becomes zero at the Brewsters angle. One possible reason is that the horizontal component of the probe's electric field alters its phase while the vertical component remains unaltered. Therefore, the phase difference $\phi_s - \phi_p$ experiences a π phase variation, and the spin accumulation would reverse its directions accordingly. This switching effect at $\delta_p = 0$ is shown in Fig. 4(c). For $\delta_p = 1.8\gamma$ similar switching happened with a less steep shift and was not shown for clarity. Due to the reversed spin-dependent splitting, the spin accumulation can be switched by slightly adjusting the incident angle near

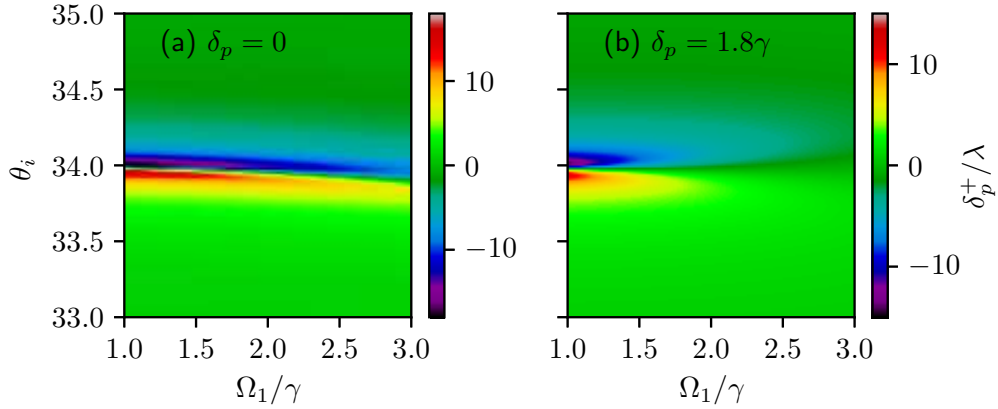


FIG. 5. (a) Contour plot of the photonic Hall shift as a function of incident angle θ_i and Ω_1 in anomalous dispersion regime $\delta_p = 0$ at fixed $\Omega_2 = 2.0\gamma$ (b) Contour plot of the photonic Hall shift as a function of incident angle θ_i and Ω_1 in normal dispersion regime $\delta_p = \Delta\nu$ at fixed $\Omega_2 = 2.0\gamma$. The rest of the parameters are unchanged.

the Brewster angle. Enhancing the ratio of r_s/r_p will result in the enhancement of the photonic spin-dependent shift δ_p^+ , which can be effectively controlled by tuning the Rabi frequencies of the control fields as long as the condition of $\Omega \gg \Omega_p$ is satisfied. This shows excellent tunability in the spectrum of spin shift by changing the strength of the control field. For incident angle θ_i , the angular width for the occurrence of the photonic SHE is $\Delta\theta = \theta^- - \theta^+$. Here, θ^+ belong to maximum positive shift while θ^- belongs to maximum negative shift. Therefore, angular width $\Delta\theta$ indicates the range of incident angles at which the Photonic spin Hall shift δ_p^+ changes sign from positive to negative. To clarify the effects of Ω and probe detuning δ_p , we extracted the $\Delta\theta$ from the results of Fig. 4 (a) and (b). Figure 4 (d) shows that angular width increases with increase of Ω . Furthermore, $\Delta\theta$ is larger for the normal dispersion regime (circles) as compared to the anomalous dispersion regime (squares).

Finally, we discuss the spin-dependent shifts in the anomalous dispersion region for $\Omega_1 \neq \Omega_2$. Our numerical results are shown in Fig. 5. In Fig. 5(a), we first fixed $\Omega_2 = 2\gamma$ and show the contour plot of the transverse SHE as a function of θ_i and Ω_1 at fixed $\delta_p = 0$. According to Fig. 5(a), the transverse SHE is positive for $\theta_i < \theta_B$ and becomes negative for $\theta_i > \theta_B$. It can be seen that the magnitudes of the positive and negative spin-dependent shifts are larger when $\Omega_1 < \Omega_2$ and the Brewster angle is also slightly shifted to lower incident angles. In Fig. 5(b), we plotted the transverse spin-separation in the normal dispersion regime $\delta_p = 1.8\gamma$. For fixed $\Omega_2 = 2\gamma$, we show the variation of the photonic SHE with respect to θ_i and Ω_1 at $\delta_p = \Delta\nu$. Again, one can see that the transverse displacements give extreme values around the Brewster's angle. If we increase the value of $\delta_p = 1.8\gamma$, then one can observe that the magnitude of the spin-dependent shift is decreasing. The shift switch sign near the Brewster's angle. Moreover, for $\Omega_1 < \Omega_2$, both the positive and negative shift mag-

nitudes are higher as shown in Fig. 5(b).

IV. CONCLUSION

In conclusion, we suggested a model for the control of the photonic Hall shift in reflected light using a three-level atomic gain medium. The photonic SHE can be enhanced as a result of a large ratio of reflection coefficients for the TE and TM modes in the presence of an atomic gain medium. By adjusting the Rabi frequencies of the control laser fields and probe field detuning, the reflection ratio can be coherently controlled, which significantly enhances photonic SHE. We have observed both positive and negative photonic SHE in anomalous and normal dispersion regimes around the Brewster angle. The range of incident angle to switch the sign of photonic SHE can be effectively controlled through the Rabi frequency of the control laser Ω . The control of photonic SHE is based on the tunable complex susceptibility via external parameters, which does not require a change of structure. Since gain-assisted superluminal light propagation has already been observed in experiments using atomic cesium vapor cell at 30°C [35]. Our proposed results may be detected in the experiment by incorporating weak measurement protocol near Brewster angle [23]. The flexible control of the spin-dependent splitting may have potential applications in cavity QED devices.

V. ACKNOWLEDGMENTS

We acknowledge the financial support from the postdoctoral research grant YS304023905 and the NSFC under Grant No. 12174346. We acknowledge fruitful discussion with Dr. M. Irfan.

-
- [1] M. Onoda, S. Murakami, and N. Nagaosa, Hall Effect of Light, *Phys. Rev. Lett.* **93**, 083901 (2004).
- [2] K. Y. Bliokh and Y. P. Bliokh, Conservation of angular momentum, transverse shift, and spin Hall effect in reflection and refraction of an electromagnetic wave packet, *Phys. Rev. Lett.* **96**, 073903 (2006).
- [3] O. Hosten and P. Kwiat, Observation of the spin Hall effect of light via weak measurements, *Science* **319**, 787 (2008).
- [4] F. Fedorov, On the polarization of electromagnetic waves, in *Dokl. Akad. Nauk SSSR*, Vol. 102 (1955) pp. 69–71.
- [5] C. Imbert, Calculation and experimental proof of the transverse shift induced by total internal reflection of a circularly polarized light beam, *Phys. Rev. D* **5**, 787 (1972).
- [6] P. Gosselin, A. Brard, and H. Mohrbach, Spin Hall effect of photons in a static gravitational field, *Phys. Rev. D* **75**, 084035 (2007).
- [7] J.-M. Mnard, A. E. Mattacchione, M. Betz, and H. M. V. Driel, Imaging the spin Hall effect of light inside semiconductors via absorption, *Opt. Lett.*, *OL* **34**, 2312 (2009).
- [8] X. Zhou, X. Ling, H. Luo, and S. Wen, Identifying graphene layers via spin Hall effect of light, *Applied Physics Letters* **101**, 251602 (2012).
- [9] L. Cai, M. Liu, S. Chen, Y. Liu, W. Shu, H. Luo, and S. Wen, Quantized photonic spin Hall effect in graphene, *Phys. Rev. A* **95**, 013809 (2017).
- [10] M. Shah, M. Shah, N. A. Khan, M. Sajid, M. Jan, and G. Xianlong, Tunable quantized spin Hall effect of light in graphene, *Results in Physics* **60**, 107676 (2024).
- [11] L. Salasnich, Enhancement of four reflection shifts by a three-layer surface-plasmon resonance, *Phys. Rev. A* **86**, 055801 (2012).
- [12] X. Zhou and X. Ling, Enhanced photonic spin Hall effect due to surface plasmon resonance, *IEEE Photonics Journal* **8**, 1 (2016).
- [13] X.-J. Tan and X.-S. Zhu, Enhancing photonic spin Hall effect via long-range surface plasmon resonance, *Opt. Lett.*, *OL* **41**, 2478 (2016).
- [14] Y. Xiang, X. Jiang, Q. You, J. Guo, and X. Dai, Enhanced spin Hall effect of reflected light with guided-wave surface plasmon resonance, *Photon. Res.*, *PRJ* **5**, 467 (2017).
- [15] R.-G. Wan and M. S. Zubairy, Controlling photonic spin Hall effect based on tunable surface plasmon resonance with an n-type coherent medium, *Phys. Rev. A* **101**, 033837 (2020).
- [16] X. Yin, Z. Ye, J. Rho, Y. Wang, and X. Zhang, Photonic spin Hall effect at metasurfaces, *Science* **339**, 1405 (2013).
- [17] M. Shah and M. Sajid, Surface states-dependent giant quantized photonic spin Hall effect in a magnetic topological insulator thin film, *Physica E: Low-dimensional Systems and Nanostructures* **138**, 115111 (2022).
- [18] M. Shah, Probing topological quantum phase transitions via photonic spin Hall effects in spin-orbit coupled 2d quantum materials, *Journal of Physics D: Applied Physics* **55**, 105105 (2021).
- [19] W. Kort-Kamp, Topological phase transitions in the photonic spin Hall effect, *Phys. Rev. Lett.* **119**, 147401 (2017).
- [20] T. Tang, K. Shen, J. Li, X. Liang, Y. Tang, C. Li, and Y. He, Optimal weak measurement scheme for chiral molecular detection based on photonic spin Hall effect, *Opt. Express*, *OE* **31**, 40308 (2023).
- [21] T. Zhu, Y. Lou, Y. Zhou, J. Zhang, J. Huang, Y. Li, H. Luo, S. Wen, S. Zhu, Q. Gong, M. Qiu, and Z. Ruan, Generalized spatial differentiation from the spin Hall effect of light and its application in image processing of edge detection, *Phys. Rev. Appl.* **11**, 034043 (2019).
- [22] Y. Qin, Y. Li, H. He, and Q. Gong, Measurement of spin Hall effect of reflected light, *Opt. Lett.*, *OL* **34**, 2551 (2009).
- [23] H. Luo, X. Zhou, W. Shu, S. Wen, and D. Fan, Enhanced and switchable spin Hall effect of light near the Brewster angle on reflection, *Phys. Rev. A* **84**, 043806 (2011).
- [24] M. O. Scully, S.-Y. Zhu, and A. Gavrielides, Degenerate quantum-beat laser: Lasing without inversion and inversion without lasing, *Phys. Rev. Lett.* **62**, 2813 (1989).
- [25] K.-J. Boller, A. Imamolu, and S. E. Harris, Observation of electromagnetically induced transparency, *Phys. Rev. Lett.* **66**, 2593 (1991).
- [26] O. Schmidt, R. Wynands, Z. Hussein, and D. Meschede, Steep dispersion and group velocity below $c/3000$ in coherent population trapping, *Phys. Rev. A* **53**, R27 (1996).
- [27] M. M. Kash, V. A. Sautenkov, A. S. Zibrov, L. Hollberg, G. R. Welch, M. D. Lukin, Y. Rostovtsev, E. S. Fry, and M. O. Scully, Ultraslow group velocity and enhanced nonlinear optical effects in a coherently driven hot atomic gas, *Phys. Rev. Lett.* **82**, 5229 (1999).
- [28] Y. Wu and L. Deng, Ultraslow optical solitons in a cold four-state medium, *Phys. Rev. Lett.* **93**, 143904 (2004).
- [29] Ziauddin, S. Qamar, and M. S. Zubairy, Coherent control of the goos-hänchen shift, *Phys. Rev. A* **81**, 023821 (2010).
- [30] L.-G. Wang, M. Ikram, and M. S. Zubairy, Control of the goos-hänchen shift of a light beam via a coherent driving field, *Phys. Rev. A* **77**, 023811 (2008).
- [31] Ziauddin, Y.-L. Chuang, and R.-K. Lee, Giant goos-hänchen shift using PT symmetry, *Phys. Rev. A* **92**, 013815 (2015).
- [32] X.-J. Zhang, H.-H. Wang, Z.-P. Liang, Y. Xu, C.-B. Fan, C.-Z. Liu, and J.-Y. Gao, Goos-hänchen shift in a standing-wave-coupled electromagnetically-induced-transparency medium, *Phys. Rev. A* **91**, 033831 (2015).
- [33] T. Shui, W.-X. Yang, Q. Zhang, X. Liu, and L. Li, Squeezing-induced giant goos-hänchen shift and hypersensitized displacement sensor in a two-level atomic system, *Phys. Rev. A* **99**, 013806 (2019).
- [34] S. Asiri and L.-G. Wang, Controlling the goos-hänchen shift in a tunable prism structure using three-level Raman gain medium, *Sci Rep* **13**, 22780 (2023).
- [35] L. J. Wang, A. Kuzmich, and A. Dogariu, Gain-assisted superluminal light propagation, *Nature* **406**, 277 (2000).
- [36] A. Dogariu, A. Kuzmich, and L. J. Wang, Transparent anomalous dispersion and superluminal light-

- pulse propagation at a negative group velocity, [Phys. Rev. A **63**, 053806 \(2001\)](#).
- [37] M. O. Scully and M. S. Zubairy, *Quantum optics* (Cambridge university press, 1997).
- [38] K. Y. Bliokh, F. J. Rodriguez-Fortuo, F. Nori, and A. V. Zayats, Spin-orbit interactions of light, [Nature Photon **9**, 796 \(2015\)](#).